



**HAL**  
open science

# Gridless three-dimensional compressive beamforming with the Sliding Frank-Wolfe algorithm

Gilles Chardon, Ulysse Boureau

► **To cite this version:**

Gilles Chardon, Ulysse Boureau. Gridless three-dimensional compressive beamforming with the Sliding Frank-Wolfe algorithm. *Journal of the Acoustical Society of America*, 2021, 150 (4), pp.3139-3148. 10.1121/10.0006790 . hal-03385213

**HAL Id: hal-03385213**

**<https://hal.science/hal-03385213v1>**

Submitted on 26 Oct 2021

**HAL** is a multi-disciplinary open access archive for the deposit and dissemination of scientific research documents, whether they are published or not. The documents may come from teaching and research institutions in France or abroad, or from public or private research centers.

L'archive ouverte pluridisciplinaire **HAL**, est destinée au dépôt et à la diffusion de documents scientifiques de niveau recherche, publiés ou non, émanant des établissements d'enseignement et de recherche français ou étrangers, des laboratoires publics ou privés.

# Gridless three-dimensional compressive beamforming with the Sliding Frank-Wolfe algorithm

Gilles Chardon<sup>1, a</sup> and Ulysse Boureau<sup>2, b</sup>

<sup>1</sup>*Université Paris-Saclay, CNRS, CentraleSupélec, Laboratoire des signaux et systèmes, 91190, Gif-sur-Yvette, France*

<sup>2</sup>*Université Paris-Saclay, CentraleSupélec, 91190, Gif-sur-Yvette, France*

(Dated: 26 October 2021)

The application of the Sliding Frank-Wolfe algorithm to gridless compressive beamforming is investigated, for single and multi-snapshots measurements, and estimation of the three-dimensional position of the sources and their amplitudes. Sources are recovered by solving an infinite dimensional optimization problem, promoting sparsity of the solutions, and avoiding the basis mismatch issue. The algorithm does not impose constraints on the source model or the array geometry. A variant of the algorithm is proposed for greedy identification of the sources. Experimental results and Monte-Carlo simulations in three dimensional settings demonstrate the performances of the method, and its numerical efficiency compared to the state of the art.

[<https://doi.org/10.1121/10.0006790>]

[XYZ]

Pages: 1–14

Copyright 2021 Acoustical Society of America. This article may be downloaded for personal use only. Any other use requires prior permission of the author and the Acoustical Society of America.

## I. INTRODUCTION

In the context of source localization<sup>1</sup>, sparsity based estimation methods offer several advantages compared to classical methods such as conventional beamforming, mostly in terms of spatial resolution and size of the data<sup>2</sup>. Sparsity based methods can be, grossly, classified in optimization based methods, mostly using the  $\ell_1$  norm<sup>3–5</sup>, or similar mixed norms<sup>6</sup>, and greedy algorithms, the most popular being Orthogonal Matching Pursuit<sup>7</sup> (OMP). These methods assume that the sources are drawn from a finite dictionary of sources, and estimate their amplitudes assuming that most of them are zero. This approach suffers from the basis mismatch problem, when actual sources cannot be exactly represented by a member of the dictionary<sup>8</sup>. It has

been shown that this problem cannot be mitigated by refining the grid: for one dimensional problems, even in low noise regimes, the LASSO method yields a number of sources doubled compared to the actual source distribution, even if sources are located on the grid<sup>9</sup>.

Several methods have been proposed to deal with this limitation. A first approach is to approximate a source at an arbitrary point by a source on a finite grid, corrected by an additional term given by a Taylor expansion. The numerical problem is then solved using sparsity based method<sup>10,11</sup>, or sparse Bayesian learning<sup>12,13</sup>.

Grid-free compressive beamforming is possible for far-field sources and uniform linear arrays<sup>14</sup>, or uniform rectangular arrays<sup>15</sup>, with possibly missing nodes or multiple snapshots<sup>16</sup>. Numerically, a finite dimensional semi-definite program (SDP)<sup>17,18</sup> is used to recover the directions of arrival. Extension to arbitrary array shapes was recently introduced<sup>19</sup>. However, other source models, such as near-field sources, cannot be tackled by this method. Finally, the Newtonized OMP (NOMP) algorithm<sup>20,21</sup> is a variant of OMP, where Newton steps are used to refine the estimations of the sources at each iteration.

---

<sup>a</sup>[gilles.chardon@centralesupelec.fr](mailto:gilles.chardon@centralesupelec.fr)

<sup>b</sup>[ulysse.boureau@student-cs.fr](mailto:ulysse.boureau@student-cs.fr)

In this paper, gridfree source localization is performed by solving the Beurling LASSO problem<sup>22</sup>, an infinite dimensional optimization problem similar to the LASSO problem. Sources are assumed to be located in a region of interest  $\Omega$ , which is here not assumed to be a discrete set. The distribution of sources is modeled by a measure  $\mu$  defined on  $\Omega$ . In the particular case of a finite number of monopolar sources, the measure  $\mu$  is a finite sum of Dirac masses, located at the positions of the sources and weighted by their amplitudes. In particular, we consider the Sliding Frank-Wolfe (SFW) algorithm<sup>23</sup> to solve the Beurling LASSO problem and estimate the positions and amplitudes of the sources.

In this algorithm, a source is added at each iteration, and the parameters of all sources are then locally and jointly optimized. Under some conditions (in particular, that the solution is a finite sum of Dirac masses, and is unique), this algorithm was shown to converge in a finite number of iterations<sup>23</sup>.

In addition to its original formulation, the SFW algorithm is here extended to deal with multi-snapshots data. Moreover, in addition to the standard SFW algorithm aiming at solving the Beurling LASSO problem, a modification of the SFW algorithm is also used as an OMP algorithm with local refinements, an alternative to NOMP. Compared to the SFW algorithm for the BLASSO problem, this variant takes the number of sources as a parameter, and its number of iterations is limited to the number of sources.

The method is demonstrated on experimental data with the localization of four sources in a 3D domain, in a case when some sources cannot be identified by beamforming because of its limited resolution. Monte-Carlo simulations are performed, to obtain results on the accuracy and computational time of the SFW algorithm, compared with previously proposed methods. While 3D localization, compared to 2D localization, does not raise fundamental challenges, practical issues arise<sup>24–26</sup>: the distance between the sources and the array is an additional parameter to be estimated, the resolution in the radial direction from the array is poorer than in the normal direction, and finally, the size of the domain of interest is increased from a surface to a volume. Therefore, efficient methods, in the sense of computational time, are necessary. The SFW based gridfree methods are shown to be

competitive, with better or equivalent estimation performances, and reduced computational complexity. Moreover, the SFW based methods do not require particular array configurations or source models.

The paper is organized as follows. Section II introduces the source localization model and discusses the state of the art. In section III, the Beurling LASSO and the SFW algorithm are recalled, and its multisnapshot variant is introduced. Numerical and experimental results are given in sections IV and V respectively. Section VI concludes the paper. The code reproducing the numerical and experimental results is available online<sup>27</sup>.

## II. MODEL AND STATE OF THE ART

We consider an array of  $M$  microphones, located at positions  $\mathbf{y}_m \in \mathbf{R}^3$  ( $m$  denoting the index of the microphone), measuring acoustical data. Complex amplitudes of the measurements at a given frequency  $f$  are obtained at times  $t_s$ , for  $s = 1 \dots S$ ,  $S$  being the number of snapshots (in practice, time domain measurements are analyzed by a Short Time Fourier Transform). Assuming the presence of  $K$  sources at positions  $\mathbf{x}_k$ , with complex amplitudes  $a_{ks}$ , the measured data  $\mathbf{p}_s \in \mathbf{C}^M$  at  $t_s$  can be decomposed as

$$\mathbf{p}_s = \sum_{k=1}^K a_{ks} \mathbf{g}(\mathbf{x}_k) + \mathbf{n}_s \quad (1)$$

where  $\mathbf{g}(\mathbf{x}_k)$  is the vector collecting the values of the Green function from the source at  $\mathbf{x}_k$  to the sensors, and  $\mathbf{n}_s$  is a measurement noise, assumed to be white in space and time. When  $S = 1$ , we write  $\mathbf{p} = \mathbf{p}_1$ , and  $a_k = a_{k1}$ . In free field conditions, the vector  $\mathbf{g}(\mathbf{x})$  is given by its coefficients

$$g_m(\mathbf{x}) = \frac{\exp(-ik\|\mathbf{x} - \mathbf{y}_m\|_2)}{\|\mathbf{x} - \mathbf{y}_m\|_2}, \quad (2)$$

where  $k = 2\pi f/c$ , with  $c$  the wave velocity. However, no particular shape is assumed for  $\mathbf{g}(\mathbf{x})$ . Our goal is to estimate the positions  $\mathbf{x}_k$  and the amplitudes  $a_{ks}$  from the measured data  $\mathbf{p}_s$ . Grid-based and grid-free methods are now recalled.

### A. Grid-based estimation

In grid based methods, the source positions  $\mathbf{x}_k$  are assumed to lie on a discrete grid of  $N$

points. A finite dimensional dictionary  $\mathbf{D} \in \mathbf{C}^{M \times N}$  is then assembled by collecting the Green functions of the grid points, and the vector of the amplitudes of the sources  $\mathbf{a} \in \mathbf{C}^N$  is recovered by solving the system

$$\mathbf{p} \approx \mathbf{D}\mathbf{a}. \quad (3)$$

The goal of sparse recovery is to find the solution of (3) with the least nonzero coefficients, i.e. with the lowest  $\ell_0$ -”norm”, defined as the number of nonzero coefficients. This problem is not tractable.

In OMP, an approximate solution of  $\ell_0$  minimization is found by selecting the sources iteratively, by identifying the source the most correlated to the data, and then by projecting the data on the orthogonal of the space spanned by the previously identified sources.

In  $\ell_1$  based approaches, the  $\ell_0$ -”norm” is replaced by its convex relaxation, the  $\ell_1$ -norm (or, in multiple snapshots settings, a mixed norm<sup>6,28</sup>). A convex minimization problem is then solved, yielding a sparse distribution of sources. The LASSO is a penalized formulation of the problem, where the vector of estimated amplitudes  $\mathbf{a}_\lambda \in \mathbf{C}^N$  is obtained by solving

$$\mathbf{a}_\lambda = \underset{\mathbf{a} \in \mathbf{C}^N}{\operatorname{argmin}} \|\mathbf{D}\mathbf{a} - \mathbf{p}\|_2^2 + \lambda \|\mathbf{a}\|_1 \quad (4)$$

where the  $\ell_1$ -norm is defined as  $\|\mathbf{a}\|_1 = \sum_{n=1}^N |a_n|$ . Alternatively, a constrained version can be used, by minimizing an  $\ell_1$ -norm under a  $\ell_2$  constraint (Basis Pursuit DeNoising, BPDN), or *vice-versa*. Application of this method to acoustical source localization was investigated in Refs.<sup>4</sup> and<sup>25</sup>.

Grid-based estimation methods are limited by the basis mismatch problem<sup>8</sup>, when a source does not exactly lie on a grid point. Then, a source is spread out over multiple grid points, hindering correct estimation of its position and amplitude.

### B. Atomic norm based compressing beamforming

In some particular cases, grid-free compressive beamforming can be achieved using finite dimensional positive semi-definite problems<sup>14,15</sup>. This is the case for far-field sources and uniform linear arrays, where  $\mathbf{g}(\mathbf{x})$  has a particular shape (that is, complex exponentials). This type of

methods is limited to specific shapes of microphone arrays and, more importantly, to the far-field case, as it takes advantage of properties of complex exponentials. This method can be extended to multiple snapshots<sup>16</sup>, and to arbitrary array shapes, using a Fourier decomposition of the measure modeling the source distribution<sup>19</sup>. However, this method imposes constraints on the model (shape of the array, far-field sources), that will not be satisfied in our numerical and experimental settings, as we consider arbitrary array shapes and non-far-field sources.

### C. OMP with local optimization

Starting from the OMP algorithm, Newtonized OMP was proposed for spectral estimation<sup>20</sup>, recently extended to source localization<sup>21</sup>. The idea of NOMP is to augment the OMP algorithm with local optimization of the positions and amplitudes of the sources, using Newton steps. To do so, sources are added at each iteration on a finite grid, and refined using a Newton optimization step, leaving other positions fixed.

After introduction of a new source, positions and amplitudes of all sources are refined one at a time, cyclically by local Newton steps, until the decrease of the energy of the residual between iterations falls below a tolerance  $\tau$ . A new iteration is then executed, with addition of a new source, until a stopping criterion is reached.

Results in two dimensional localization showed that estimation of the positions of the sources was improved compared to OMP, using the same finite grid<sup>21</sup>. However, the method fails with coarse grids, when local Newton iterations do not converge towards a local minimum of the objective function<sup>20</sup>.

### D. Block sparsity with Taylor approximations

Block-sparsity, combined with Taylor approximations, can be used for grid-free sparse estimation. With  $\mathbf{z}$  a member of the grid, an off-grid source at position  $\mathbf{z} + \Delta$ , with offset  $\Delta = (\Delta_x, \Delta_y, \Delta_z)$ , of amplitude  $a$  can be approximated as

$$a\mathbf{g}(\mathbf{z} + \Delta) \approx a\mathbf{g}(\mathbf{z}) + a\Delta_x \frac{\partial \mathbf{g}}{\partial x} + a\Delta_y \frac{\partial \mathbf{g}}{\partial y} + a\Delta_z \frac{\partial \mathbf{g}}{\partial z}. \quad (5)$$

For positive real amplitudes  $a$ , off-grid sources can be localized by the Continuous Basis Pursuit method<sup>10</sup>, minimization of the  $\ell_1$  norm of the sources with additional convex constraints on the corrections, ensuring that they remain bounded by  $\delta/2$ , with  $\delta$  the grid step. However, it was shown that for small grid steps  $\delta$ , this method, as the finite dimensional LASSO, represents a unique source by multiple grid points<sup>29</sup>. For complex amplitudes, the constraints necessary to ensure that the corrections are not larger than  $\delta/2$  are non-convex. In this case, a mixed-norm can be used<sup>11</sup>. For each grid point, a vector of amplitudes  $(\hat{a}_0, \hat{a}_1, \hat{a}_2, \hat{a}_3) \approx (a, a\Delta_x, a\Delta_y, a\Delta_z)$  (most of them begin null) is estimated, from which the correction of the position is obtained. However, compared to the positive real amplitudes case, this formulation does not ensure that the corrected point stays near the associated grid point (in fact, the quotients  $\hat{a}_{1,2,3}/\hat{a}_0$  are, in general, complex). Finally, the step  $\delta$  has to be small enough so that the linear approximation around the center of a cell remains precise enough in the cell, implying small steps  $\delta$  and large computational grids.

### III. THE SLIDING FRANK-WOLFE ALGORITHM

We introduce now the Beurling LASSO problem, and the Sliding Frank-Wolfe algorithm used to solve it. Assuming that the sources are located in a region of interest  $\Omega$ , the distribution of sources is modeled by a measure  $\mu$ , i.e. a function taking as input a subset<sup>30</sup> of  $\Omega$ , yielding a positive, real, or complex value (resp measure, signed measure, and complex measure). The measure  $\mu$  models the distribution of sources in the domain of interest  $\Omega$ , without the need of a discrete grid.

A particular example of measure is the Dirac mass  $\delta_{\mathbf{x}}$  which can be used to model a point source at position  $\mathbf{x} \in \Omega$  of unit amplitude. We recall that the integral of a function  $f$  with respect to the Dirac mass  $\delta_{\mathbf{x}}$  is given by

$$\int_{\Omega} f d\delta_{\mathbf{x}} = f(\mathbf{x}). \quad (6)$$

In general, a distribution of  $K$  sources at time  $t_s$  with positions  $\mathbf{x}_k$  and complex amplitudes  $a_{ks}$  is modeled by the discrete measure

$$\mu_s = \sum_{k=1}^K a_{ks} \delta_{\mathbf{x}_k}. \quad (7)$$

Equation (1) can be rewritten as

$$\mathbf{p}_s = \int_{\Omega} \mathbf{g} d\mu_s + \mathbf{n}_s. \quad (8)$$

The source localization method introduced in this paper is based on the Sliding Frank-Wolfe algorithm<sup>23</sup>, which aims at solving the Beurling LASSO problem, which is defined for  $S = 1$  by

$$\mu^* = \operatorname{argmin}_{\mu \in \mathcal{M}} \frac{1}{2} \left\| \int_{\Omega} \mathbf{g} d\mu - \mathbf{p} \right\|^2 + \lambda |\mu|(\Omega) \quad (9)$$

where  $\mathcal{M}$  is the set of complex measures defined on  $\Omega$ . Then, positions and amplitudes of the sources are given by the decomposition of  $\mu^*$  in (7).

The regularization term  $|\mu|(\Omega)$  is the total variation norm of the complex measure  $\mu$ , defined by<sup>31</sup>

$$|\mu|(\Omega) = \max_{f \in C_1} \int_{\Omega} f d\mu \quad (10)$$

where  $C_1$  is the set of continuous functions on  $\Omega$  with absolute value bounded by 1. For a discrete measure  $\mu = \sum_{k=1}^K a_k \delta_{\mathbf{x}_k}$  (with pairwise distinct  $\mathbf{x}_k$ ), the definition reduces to

$$|\mu|(\Omega) = \sum_{k=1}^K |a_k|. \quad (11)$$

We observe that we recover here the  $\ell_1$  norm of the amplitudes of the sources. It can also be considered as the atomic norm of  $\mu$  using Dirac masses as building blocks. The Beurling LASSO is similar to the LASSO problem (4), with the important difference that positions of the estimated sources are not limited to a predefined finite grid.

The SFW algorithm solves problem (9) by iteratively adding Dirac masses to the measure being optimized, alternating with local updates of the positions and amplitudes of the Dirac masses. The steps of the algorithm are given in detail in Algorithm 1. The notation  $\mathbf{G}(\mathbf{X})$  denotes the  $M \times k$  matrix collecting the values of  $\mathbf{g}$  for the positions in the tuple  $\mathbf{X} = (\mathbf{x}_1, \dots, \mathbf{x}_k)$ .  $()$  denotes the empty tuple, and  $(\mathbf{X}, \mathbf{x}_*)$  the insertion of  $\mathbf{x}_*$  into the tuple  $\mathbf{X}$ .  $K_{\max}$  is the maximal number of iterations. An iteration consists of the following steps:

- firstly, a source is added by solving the global optimization problem (12). To this end, the maximum of  $\eta^{[k]}$  (defined in (13)) is searched on a finite grid, and used as initialization for a local optimization.
- Amplitudes are then updated in problem (14), a LASSO problem.
- Finally, amplitudes and positions are jointly optimized in problem (15). This problem is non-convex (indeed, the objective function is left unchanged by permutation of the positions and amplitudes of two sources, and replacing the positions and amplitudes of these two sources by their mean is unlikely to yield a lower value of the objective function as would be the case for a convex objective function). However, local optimization is sufficient, e.g. with a quasi-Newton algorithm, initialized at positions  $\mathbf{X}^{[k-1/2]}$  and amplitudes  $\mathbf{a}^{[k-1/2]}$ .

Under some constraints on the solution  $\mu^*$  (in particular, that it is a finite sum of Dirac masses), the algorithm is shown to converge in a finite number of iterations<sup>23</sup>. In our implementation, the Matlab 2019b function `fmincon` was used to solve problems (12), (14) and (15), using the sequential quadratic programming algorithm<sup>32</sup>.

#### A. Multi-snapshots data

In this subsection, we present a modification of the SFW algorithm aimed at processing multi-snapshot data. In the case of several snapshots, the measured data  $\mathbf{p}_s$  is assembled in the  $M \times S$  matrix  $\mathbf{P}$ . Amplitudes for each source and each snapshot are optimized in problems (14) and (15). In problem (15), positions of the sources are common among the snapshots. In these problems, the  $\ell_1$ -norm is replaced by a mixed-norm<sup>6,28</sup>. With  $\mathbf{A}$  the  $k \times S$  matrix containing the complex amplitudes of  $k$  sources for  $S$  snapshots, and each row  $\mathbf{a}_{r,j}$  corresponding to the amplitudes of the  $j$ -th source for the  $S$  snapshots, we define the  $\ell_{2,1}$  mixed norm as

$$\|\mathbf{A}\|_{2,1} = \sum_{j=1}^k \|\mathbf{a}_{r,j}\|_2. \quad (16)$$

In a given row, the  $\ell_2$  norm is considered, which does not impose sparsity inside the row. Indeed, this would imply temporal sparsity of the source,

ALGORITHM 1: Sliding Frank-Wolfe algorithm, solving problem (9)

---



---

$\mu^{[0]} \leftarrow 0, \mathbf{r}^{[0]} \leftarrow \mathbf{p}, \mathbf{X}^{[0]} \leftarrow ()$

**for**  $k = 1, \dots, K_{\max}$  **do**

    Identify a new source by solving

$$\mathbf{x}_* = \operatorname{argmax}_{\mathbf{x} \in \Omega} \eta^{[k]}(\mathbf{x}) \quad (12)$$

    where

$$\eta^{[k]}(\mathbf{x}) = \frac{1}{\lambda} |g(\mathbf{x})^* \mathbf{r}^{[k-1]}| \quad (13)$$

**if**  $\eta(\mathbf{x}_*) \leq 1$  **then**

        Stop

**else**

$\mathbf{X}^{[k-1/2]} = (\mathbf{X}^{[k]}, \mathbf{x}_*)$

        Optimize the amplitudes:

$$\mathbf{a}^{[k-1/2]} = \operatorname{argmin}_{\mathbf{a} \in \mathbf{C}_+^k} \frac{1}{2} \|\mathbf{G}(\mathbf{X}^{[k-1/2]})\mathbf{a} - \mathbf{p}\|_2^2 + \lambda \|\mathbf{a}\|_1 \quad (14)$$

        Optimize the amplitudes and positions:

$$(\mathbf{X}^{[k]}, \mathbf{a}^{[k]}) = \operatorname{argmin}_{\mathbf{X} \in \Omega^k, \mathbf{a} \in \mathbf{C}_+^k} \frac{1}{2} \|\mathbf{G}(\mathbf{X})\mathbf{a} - \mathbf{p}\|_2^2 + \lambda \|\mathbf{a}\|_1 \quad (15)$$

$\mu^{[k]} \leftarrow \sum_{n=1}^k a_n^{[k]} \delta_{\mathbf{x}_n^{[k]}}$ ,  $\mathbf{r}^{[k]} \leftarrow \mathbf{p} - \mathbf{G}(\mathbf{X}^{[k]})\mathbf{a}^{[k]}$

**end if**

**end for**

---



---

which is not expected here. Then, the  $\ell_1$  norm of the  $\ell_2$  norms is computed, as we expect spatial sparsity.

The function  $\eta$  is updated, with

$$\eta^{[k]}(\mathbf{x}) = \frac{1}{\lambda} \sqrt{\sum_{s=1}^S \left| \mathbf{g}(\mathbf{x})^* \mathbf{r}_s^{[k-1]} \right|^2} \quad (17)$$

where  $\mathbf{r}_s^{[k-1]}$  is the residual for the  $s$ -th snapshot, defined by

$$\mathbf{r}_s^{[k]} = \mathbf{p}_s - \mathbf{G}(\mathbf{X}^{[k]})\mathbf{a}_{c,s}^{[k]}, \quad (18)$$

$\mathbf{a}_{c,s}^{[k]}$  being the  $s$ -th column of  $\mathbf{A}^{[k]}$ , containing the amplitudes of the sources for the  $s$ -th snapshot. Details on this choice of  $\eta$  are given in the Appendix.

Problems (14) and (15) are replaced by:

$$\mathbf{A}^{[k-1/2]} = \operatorname{argmin}_{\mathbf{A} \in \mathbf{C}^{kS}} \frac{1}{2} \|\mathbf{G}(\mathbf{X}^{[k-1/2]})\mathbf{A} - \mathbf{P}\|_F^2 + \lambda \|\mathbf{A}\|_{2,1} \quad (19)$$

and

$$(\mathbf{X}^{[k]}, \mathbf{A}^{[k]}) = \underset{\mathbf{X} \in \Omega^k, \mathbf{A} \in \mathbf{C}^{k \times S}}{\operatorname{argmin}} \frac{1}{2} \|\mathbf{G}(\mathbf{X})\mathbf{A} - \mathbf{P}\|_{\mathbb{F}}^2 + \lambda \|\mathbf{A}\|_{2,1} \quad (20)$$

where  $\|\cdot\|_{\mathbb{F}}$  denotes the Frobenius norm of a matrix, defined as the  $\ell_2$  norm of its coefficients.

### B. Setting the regularization parameter $\lambda$

Setting the regularization parameter is known to be a difficult problem. To help this tuning, the homotopy approach can be used<sup>33</sup>: results of the algorithm for several parameters  $\lambda$  can be obtained by sequentially running the SFW algorithm for decreasing  $\lambda$ , initializing each run with the output of the previous run. In this case, the algorithm starts by solving (15) and checking the value of  $\eta$ , to avoid addition of a source if not necessary. The search of the parameter  $\lambda$  can be stopped when an appropriate number of sources is found, or according to Morozov's principle<sup>34</sup>, by setting  $\lambda$  such that the error between the measurements and the acoustical field generated by the estimated sources  $\|\mathbf{G}(\mathbf{X})\mathbf{A} - \mathbf{P}\|_{\mathbb{F}}^2$  is in the order of the expected noise level.

### C. A greedy version of SFW

While the SFW algorithm solves a minimization problem, its structure is similar to greedy sparse recovery algorithms such as OMP. The SFW algorithm can be used for greedy identification of acoustical sources by setting  $\lambda = 0$ , using a normalized dictionary  $\mathbf{g}_n(\mathbf{x}) = \mathbf{g}(\mathbf{x})/\|\mathbf{g}(\mathbf{x})\|_2$ , and stopping the algorithm after a fixed number of iterations. This version of SFW is more practical when an estimation of the number of sources is known. Moreover, the number of iterations is limited to the iterations necessary to recover the sources, whereas additional spurious sources can slow the algorithm down, because of the additional iterations and the higher number of parameters to optimize in problems (14) and (15).

Compared to NOMP, where positions and amplitudes of the sources are optimized sequentially, at each iteration, here positions and amplitudes of all identified sources are locally and jointly optimized. The normalized dictionary  $\mathbf{g}_n$  will also be used when solving the BLASSO problem (9).

## IV. NUMERICAL RESULTS

Performances of the SFW algorithm for acoustical source localization, in comparison to the state of the art, are now assessed using simulated data. Both versions of SFW are considered: *penalized SFW*, solving problem (9), and *greedy SFW*, introduced in subsection III C.

### A. A simple 1D example

To allow comparison between the semi-definite programming based method, BPDN, block-sparsity, penalized SFW, a first simulation is made in the case of a simple one dimensional direction of arrival estimation. Results of ESM-IRLS<sup>24</sup> are also given.

Figure 1 shows the result of localization of two far field sources of amplitudes 1 and 2 Pa, arriving from angles  $\theta_1 = 0.21$  and  $\theta_2 = -0.53$ , with a uniform linear array of 20 microphones with pitch half the wavelength, using  $S = 1$  snapshot. For the SDP problem, BPDN and block-sparsity estimation, the tolerance  $\epsilon$  is set as twice the norm of the noise, and for SFW,  $\lambda = 1$ . ESM-IRLS<sup>24</sup> is used with  $p = 0$ . The grid used for BPDN, block-sparsity and ESM-IRLS, and to initialize problem (12) in SFW, is a regular sampling of 40 values of  $\sin(\theta)$  in the interval  $[-\pi/2, \pi/2]$ . For block-sparsity, the derivative of the dictionary is normalized so that the decomposition of a source located between grid points has coefficients in the dictionary and its derivative of the same order.

Although  $\theta_1$  and  $\theta_2$  are not on the grid, SDP and SFW are capable of estimating the directions of arrival correctly. For BPDN, block-sparsity and EMS-IRLS, each source is represented by two spikes. Moreover, several spurious sources appear, caused by the basis mismatch.

### B. Performances of the SFW algorithm

Now, performances of the SFW algorithm, in its original penalized version (*SFW p.*) and greedy version (*SFW g.*), OMP, and NOMP are compared, in function of several parameters: step  $\delta$  of the discretization grid, frequency, SNR, number of snapshots, and resolution, using Monte-Carlo simulations. The SDP based grid-free method cannot be used here, as it cannot deal with the source model. The block-sparsity method was also considered, but long running

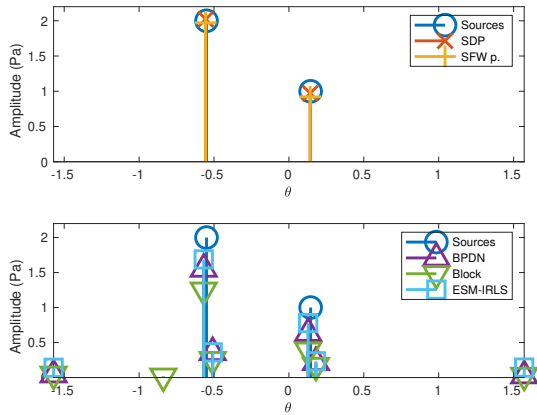


FIG. 1. Simulations. Direction of arrival estimation, (a) SFW and SDP, (b) BPDN and block sparsity (amplitudes below  $10^{-2}$  are not plotted). (color online)

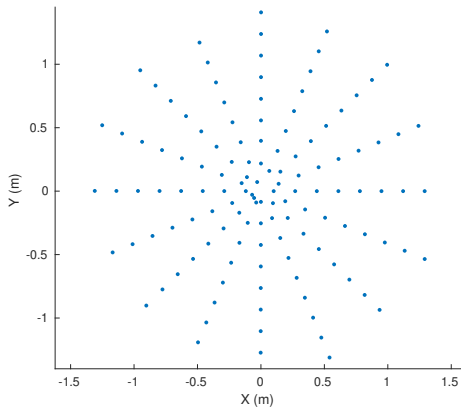


FIG. 2. Layout of the microphone array

times (typical running times of 500s compared to less than a second for the greedy SFW algorithm at  $\delta = 0.1\text{m}$ ) prevented its use in the simulations. An array of 128 microphones is used, with positions of the microphones shown on figure 2 in the plane  $Z = 0$ . The domain  $\Omega$  is defined by  $-1 \leq X \leq 1$ ,  $-1 \leq Y \leq 1$ ,  $3 \leq Z \leq 5$  (in meters), discretized with a step  $\delta = 0.05\text{m}$  (except when stated otherwise). Three sources are randomly placed in  $\Omega$  using a uniform density, with amplitudes 0.1 Pa, 0.2 Pa and 0.4 Pa resp., and random phases. For the original SFW algorithm, the  $\lambda$  parameter is chosen as the minimal value such that three sources are identified. Estimated amplitudes obtained by least-squares fitting of the data to the sources identified by the BLASSO problem, avoiding the bias introduced

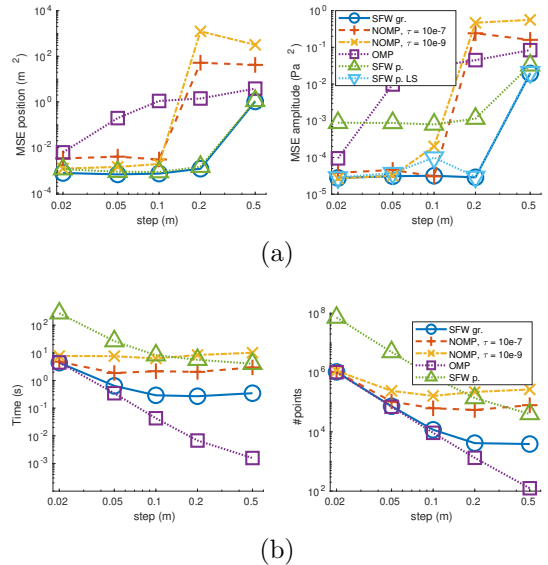


FIG. 3. Simulations. Performances of greedy SFW, penalized SFW, OMP and NOMP, in function of the grid step. (a) MSE in position (left) and amplitude (right), (b) computational time (left) and number of positions visited (right). (color online)

by the regularization terms, are also given (*SFW p. LS*).

50 realizations of the data are used to estimate the Mean Square Error (MSE) of the positions and amplitudes of the sources.

*a. Grid step.* In OMP, estimated positions will necessarily lie on the grid, while for NOMP and SFW, the grid is used only at the identification step, followed by local optimization, and should have a lesser impact on the localization results.

MSE for the position and amplitude estimation are given on figure 3-(a), for OMP, NOMP with tolerances  $\tau = 10^{-7}$  and  $\tau = 10^{-9}$ , and SFW, with  $S = 1$ ,  $F = 4858\text{Hz}$  and a SNR of 20dB. As expected, performances of OMP worsen as the step increases. Compared to OMP, the local optimization of NOMP with  $\tau = 10^{-7}$  improves the localization performances. NOMP with  $\tau = 10^{-9}$  reaches similar performances to SFW for steps up to 0.1m. However, at  $\delta = 0.2\text{m}$ , performances of NOMP degrades, compared to SFW. This can be explained by the fact that the condition for convergence of the Newton method towards a local maximum of the likelihood function are not satisfied<sup>20</sup>: at the grid point where a source is first placed, the objec-

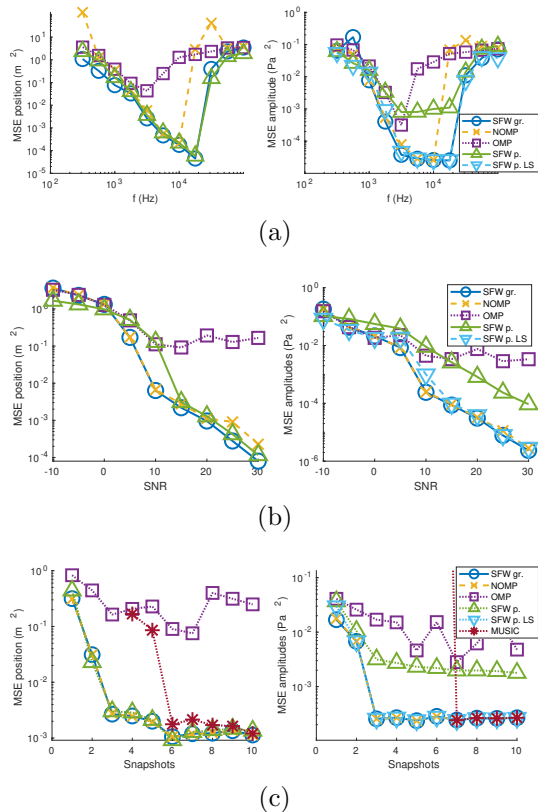


FIG. 4. Simulations. Position (left) and amplitude MSE (right) in function of (a) frequency  $F$ , (b) SNR, (c) number of snapshots  $S$ . (color online)

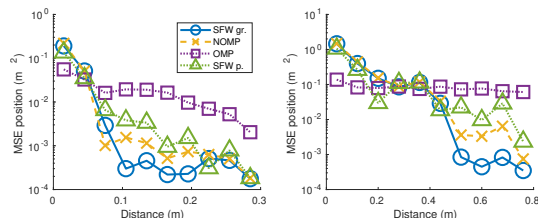


FIG. 5. Simulations. Position MSE in the case of two sources with varying distance, with sources in the same plane parallel to the array (left), and in the same axis normal to the array (right). (color online)

tive function is non-convex, and the Newton step does not yield a relevant update of the position. For larger steps, SFW also fails. Here, the grid is too coarse compared to the wavelength to allow to initialize the optimization problem (12) near the global optimum.

Amplitude estimated by solving the Beurling LASSO problem with the penalized SFW algo-

rithm are biased. Reestimating the amplitudes improve the estimation of the amplitudes.

For the following numerical experiments, the tolerance  $\tau = 10^{-9}$  will be used for NOMP.

**b. Frequency.** Performances with respect to the frequency are plotted on figure 4-(a), with  $S = 1$ , a grid step of 0.05m, and a SNR of 20dB. At low frequencies, the methods can return several sources with identical positions when the distance between sources is not sufficient. In this case, estimation of the amplitude of the sources is ill-conditioned. To avoid large error in amplitude estimations cause by this ill-conditioning, when two sources have estimated position  $\mathbf{x}$  and  $\mathbf{x}'$  such that  $|\langle \mathbf{g}(\mathbf{x}), \mathbf{g}(\mathbf{x}') \rangle| / (\|\mathbf{g}(\mathbf{x})\| \|\mathbf{g}(\mathbf{x}')\|) > 0.98$ , their amplitudes are replaced by their averages, and similarly when the three sources are estimated at the same position.

Here, it is expected that the performances improve with increasing frequencies. This improvement is visible for all methods at lower frequencies (performances of OMP are however limited by the coarse grid used here). Above frequency 10kHz for NOMP, and 18kHz for SFW, performances of the methods degrade. This failure is explained as in the case of varying grid step, by the coarseness of the grid compared to the wavelength.

**c. SNR.** Here, we analyze the effect of the noise level on the estimation. Figure 4-(b) shows the MSE in position and amplitudes with respect to the SNR, with  $S = 1$ ,  $F = 4858\text{Hz}$ . Performances of OMP are limited by the grid. NOMP and greedy SFW show similar performances except at high SNR. This discrepancy is caused by stopping the local optimization of NOMP when the tolerance  $\tau$  is reached, before convergence.

**d. Number of snapshots.** The performances of the methods are now compared for increasing number of snapshots, from  $S = 1$  to  $S = 10$ , with  $F = 4858\text{Hz}$  and a SNR of 10dB, on Figure 4-(c). Here, the amplitudes of the sources at each snapshot are drawn from independent random complex Gaussian variables, such that their RMS amplitudes are 0.1 Pa, 0.2 Pa and 0.4 Pa resp.. All methods fail for a unique snapshot. This is caused by the lower SNR, and the random amplitudes, which thus can be close to zero for some sources in some configurations. Using several snapshots ensures that all sources have a sufficient amplitude for at least one snapshot. Results of the MUSIC algorithm are also given

when the number of snapshots is larger than the number of sources, showing better performances of SFW compared to MUSIC, for the values of  $S$  used here.

*e. Resolution.* Finally, the resolution of the methods is compared. Two sources of identical amplitudes are used with  $S = 1$ ,  $F = 4858\text{Hz}$ , and SNR of 20dB, with varying distance between the sources. Figure 5 shows the position error when the two sources are in a plane parallel to the array (left panel), and with the two sources have identical  $X$  and  $Y$  coordinates (right panel). Greedy SFW, penalized SWF and NOMP improve at the same threshold (approx. 0.075m in the  $XY$  plane and 0.44m in the  $Z$  axis). Greedy SFW exhibits better performances for distances up to twice this threshold.

*f. Computational effort.* On figure 3-(b), the computational time (on a personal laptop equipped with an Intel Core i7-7820HQ @ 2.90GHz  $\times$  8 CPU and 16 GB memory) of the four methods is plotted, as well as the number of positions  $\mathbf{x}$  where  $\mathbf{g}(\mathbf{x})$  is computed, for varying grid step. SFW yields results in a shorter time than NOMP at  $\tau = 10^{-9}$  by an order of magnitude, with fewer visited positions. This discrepancy is, in part, explained by the fact that SFW optimizes the positions and amplitudes of all sources jointly, while NOMP considers them separately.

In conclusion, these numerical experiments show that the SFW algorithm compares favorably with respect to the NOMP method. Indeed, when both methods succeed in locating the sources, the SFW algorithm yields similar or better performances than NOMP. Additionally, the SFW algorithm does not necessitate grids as fine as NOMP. At fixed grid size, NOMP shows higher computational times at a tolerance  $\tau$  yielding similar performances to SFW. These observations show that the SFW algorithm is better suited than NOMP for gridfree source localization, in particular at high frequencies, as the necessary grid step scales like the wavelength. The greedy version of SFW was found to yield slightly better performances than the SFW algorithm solving BLASSO problem, even after re-estimation of the amplitudes.

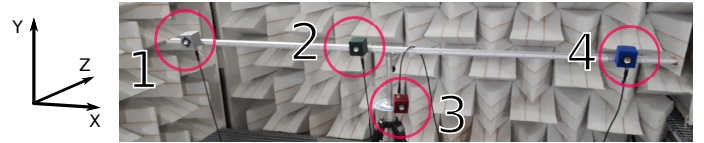


FIG. 6. Acoustical sources and coordinate frame. (color online)

## V. EXPERIMENTAL RESULTS

In the experimental results, four sources (Visaton-BF32 omnidirectional loudspeakers) are used, pictured on Fig. 6, emitting white noise. The acoustical field is measured using an array of 128 MEMS microphones (IN-VESENSE-INMP441), with positions shown on Fig. 2. The sampling frequency is  $F_s = 50$  kHz, and signals are analyzed by a Short-Time Fourier Transform, with Hann window of duration 82ms (4096 samples) and 50% overlap. More details on the experimental setup are found in Ref.<sup>35</sup>.

The domain of interest is the box defined by  $-2 \leq X \leq 1$ ,  $-1 \leq Y \leq 0$ ,  $4 \leq Z \leq 5$  (in meters), containing the four sources.  $S = 10$  snapshots are used, and results are obtained at frequency  $F = 1818\text{Hz}$ . Results of conventional beamforming are given on Figure 9-(a). At the chosen frequency, the two central sources cannot be separated by beamforming.

The penalized SFW algorithm is run for several values of  $\lambda$  in the BLASSO problem (9) using the homotopy approach described in subsection III B, with the normalized dictionary  $\mathbf{g}_n$ . Estimated amplitudes and positions of the sources depend on the regularization parameter  $\lambda$ . Fig. 7 shows the evolution of the estimated amplitudes of the sources in function of  $\lambda$ . Amplitudes are defined as the root mean square of the amplitudes for each snapshot, normalized by the amplitude of the most powerful source, estimated by beamforming from measurements where it is the only active source. Each color represents a source identified by the algorithm. For high  $\lambda$ , amplitudes of the sources are underestimated, while for low  $\lambda$ , several spurious sources appear.

Figure 8 highlights the importance of the normalization of the dictionary. Here, the estimated  $Z$  coordinates for each source are plotted in function of the regularization parameter  $\lambda$ , using the un-normalized dictionary  $\mathbf{g}$  and the

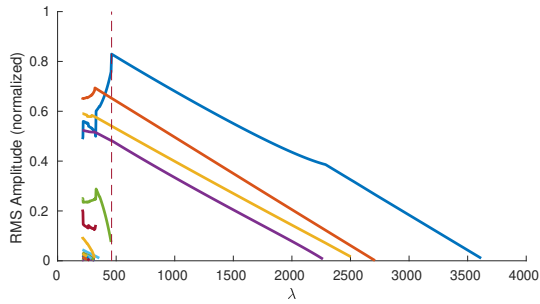


FIG. 7. Experimental results. Root mean square amplitudes of the sources (identified by a color) found by penalized SFW with the normalized dictionary  $\mathbf{g}_n$ , in function of the regularization parameter  $\lambda$ . The parameter  $\lambda$  used in Fig. 9 is indicated by the dashed line. (color online)

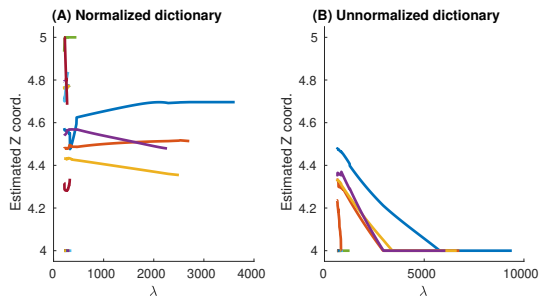


FIG. 8. Experimental results.  $Z$ -coordinate of the sources identified by penalized SFW for the normalized  $\mathbf{g}_n$  and un-normalized model  $\mathbf{g}$ , in function of the regularization parameter  $\lambda$ . (color online)

$\ell_2$ -normalized dictionary  $\mathbf{g}_n$ . Using  $\mathbf{g}$ , estimated positions are biased towards the array for large  $\lambda$ . Indeed, in these cases, it is preferable to estimate a source at a position closer to the array, where the model does not match the data as well as the correct position, but the necessary amplitude is smaller, and therefore generates a smaller penalization. While estimated  $Z$  coordinates fluctuate in function of  $\lambda$  when using  $\mathbf{g}_n$ , no clear bias is visible.

On figure 9, estimated positions for  $\lambda = 648$  (just before the appearance of a fifth source, denoted as penalized SFW) are plotted. On this same figure, results of the greedy version of SFW, OMP, NOMP (the data-dependent tolerance  $\tau$  is here  $\tau = 0.01$ , which has been observed to yield similar results to SFW), MUSIC and CSCD combined with ESM-IRLS<sup>24</sup> are reported, with four iterations.

Estimated powers of the sources are given in table I for OMP, NOMP, greedy and penalized SFW, and MUSIC, and are compared to the power estimated by beamforming, in settings where each source is the unique active source.

## VI. CONCLUSION

The application of the Sliding Frank-Wolfe algorithm for acoustical source localization is introduced. Modifications of the algorithm were used, to take into account multi-snapshots data, and perform greedy identification of the sources. Estimation performances were shown to be better, or comparable, than the state of the art. Additionally, the method is numerically efficient, with smaller computational times than other grid-free methods, and is not based on a particular source model or limited to specific array shapes. Results for several values of the regularization parameter  $\lambda$  are obtained, helping the choice of the regularization parameter.

## ACKNOWLEDGMENTS

The authors thank François Ollivier (Institut d'Alembert, Sorbonne Université, CNRS) for making the experimental results possible.

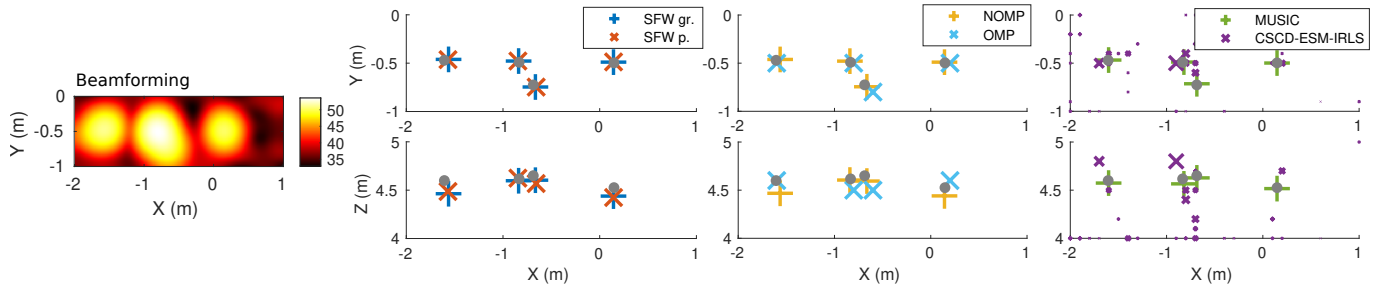


FIG. 9. Experimental results. Beamforming in a plane, and. Greedy and penalized versions of SFW, OMP, NOMP, MUSIC and CSCD-ESM-IRLS. Front (top) and top (bottom) views. Size of the markers is proportional to source power. (color online)

	Power	OMP	NOMP	SFW gr.	SFW p.	SFW p. LS	MUSIC
Source 1	52.9	51.8	51.6	51.5	50.0	51.6	51.7
Source 2	53.3	53.5	53.4	53.4	52.0	53.4	53.6
Source 3	51.0	48.1	49.6	49.6	47.3	49.5	50.1
Source 4	50.8	50.1	50.1	50.1	48.3	50.1	50.3

TABLE I. Experimental results. Estimated powers of the sources for OMP, NOMP, greedy SFW, penalized SFW (penal. SFW), and penalized SFW with least-squares estimation of the amplitudes (penal. SFW LS).

## APPENDIX A: SELECTION CRITERION $\eta$

In Algorithm 1,  $\eta^{[k]}$  is defined as

$$\eta^{[k]}(\mathbf{x}) = \frac{1}{\lambda} |\mathbf{g}(\mathbf{x})^* \mathbf{r}^{[k-1]}|. \quad (\text{A1})$$

At the end of an iteration, where amplitudes and positions of the estimated sources are locally optimal, the objective function can be locally improved only by adding a new source. Defining  $h_{\mathbf{x},\psi}(\epsilon) = J(\mu^k + \epsilon e^{i\psi} \delta_{\mathbf{x}}) - J(\mu^k)$  the variation of the objective function  $J$  of problem (9) when introducing a source at  $\mathbf{x}$  with phase  $\psi$  and positive amplitude  $\epsilon$ ,

$$h'_{\mathbf{x},\psi}(0) = -\text{Re}(e^{-i\psi} \mathbf{g}(\mathbf{x})^* \mathbf{r}^{[k-1]}) + \lambda. \quad (\text{A2})$$

Maximal decrease is obtained when  $\psi$  is chosen as the angle  $\psi_*$  of  $(\mathbf{g}(\mathbf{x})^* \mathbf{r}^{[k-1]})^*$ , yielding

$$h'_{\mathbf{x},\psi_*}(0) = -|\mathbf{g}(\mathbf{x})^* \mathbf{r}^{[k-1]}| + \lambda. \quad (\text{A3})$$

Maximizing  $\eta^{[k]}(\mathbf{x})$  can therefore be interpreted as choosing the position  $\mathbf{x}$  where adding a source maximizes the improvement of the objective function. Moreover, when  $h'_{\mathbf{x},\psi_*}(0) \geq 0$  for all possible positions  $\mathbf{x}$  (equivalently,  $\eta^{[k]}(\mathbf{x}) \leq 1$ ), the objective function cannot be improved by adding a source, and the algorithm stops.

For the multsnapshot problem, we define  $h_{\mathbf{x},\mathbf{u}}(\epsilon)$  as the variation of the objective function when a source is introduced at  $\mathbf{x}$  with amplitudes  $u_s \epsilon$  for each snapshot, with  $\|\mathbf{u}\|_2 = 1$  and  $\epsilon \geq 0$ . Then

$$h'_{\mathbf{x},\mathbf{u}}(0) = -\sum_{s=1}^S \text{Re}((u_s \mathbf{g}(\mathbf{x}))^* \mathbf{r}_s^{[k-1]}) + \lambda \quad (\text{A4})$$

Defining  $\mathbf{v}$  such that  $v_s = \mathbf{g}(\mathbf{x})^* \mathbf{r}_s^{[k-1]}$ ,

$$h'_{\mathbf{x},\mathbf{u}}(0) = -\text{Re}(\mathbf{u}^* \mathbf{v}) + \lambda. \quad (\text{A5})$$

The vector  $\mathbf{u}$  maximizing the decrease of the objective function for a given position  $\mathbf{x}$  is obtained by choosing  $\mathbf{u}$  colinear with  $\mathbf{v}$ , that is  $\mathbf{u}_* = \mathbf{v} / \|\mathbf{v}\|_2$ , and

$$h'_{\mathbf{x},\mathbf{u}_*}(0) = -\|\mathbf{v}\|_2 + \lambda \quad (\text{A6})$$

We then define

$$\eta(\mathbf{x}) = \|\mathbf{v}\|_2 / \lambda \quad (\text{A7})$$

with  $\eta(\mathbf{x}) \leq 1$  when the objective function cannot be decreased by adding a source.

<sup>1</sup>H. Krim and M. Viberg, “Two decades of array signal processing research: the parametric approach,” *IEEE Signal Processing Magazine* **13**(4), 67–94 (1996) doi: [mu10.1109/79.526899](https://doi.org/10.1109/79.526899).

<sup>2</sup>P. Gerstoft, C. F. Mecklenbräuker, W. Seong, and M. Bianco, “Introduction to compressive sensing in acoustics,” *The Journal of the Acoustical Society of America* **143**(6), 3731–3736 (2018) [muhttp://asa.scitation.org/doi/10.1121/1.5043089](https://doi.org/10.1121/1.5043089) doi: [mu10.1121/1.5043089](https://doi.org/10.1121/1.5043089) publisher: Acoustical Society of America.

<sup>3</sup>S. S. Chen, D. L. Donoho, and M. A. Saunders, “Atomic Decomposition by Basis Pursuit,” *SIAM Review* **43**(1), 129–159 (2001) [muhttps://epubs.siam.org/doi/10.1137/S003614450037906X](https://epubs.siam.org/doi/10.1137/S003614450037906X) doi: [mu10.1137/S003614450037906X](https://doi.org/10.1137/S003614450037906X) publisher: Society for Industrial and Applied Mathematics.

<sup>4</sup>P. Simard and J. Antoni, “Acoustic source identification: Experimenting the  $\ell_1$  minimization approach,” *Applied Acoustics* **74**(7), 974–986 (2013) doi: [mu10.1016/j.apacoust.2013.01.012](https://doi.org/10.1016/j.apacoust.2013.01.012).

<sup>5</sup>A. Xenaki, P. Gerstoft, and K. Mosegaard, “Compressive beamforming,” *The Journal of the Acoustical Society of America* **136**(1), 260–271 (2014) [muhttp://asa.scitation.org/doi/10.1121/1.4883360](https://asa.scitation.org/doi/10.1121/1.4883360) doi: [mu10.1121/1.4883360](https://doi.org/10.1121/1.4883360).

<sup>6</sup>D. Malioutov, M. Cetin, and A. Willsky, “A sparse signal reconstruction perspective for source localization with sensor arrays,” *IEEE Transactions on Signal Processing* **53**(8), 3010–3022 (2005) doi: [mu10.1109/TSP.2005.850882](https://doi.org/10.1109/TSP.2005.850882).

<sup>7</sup>Y. Pati, R. Rezaifar, and P. Krishnaprasad, “Orthogonal matching pursuit: recursive function approximation with applications to wavelet decomposition,” in *Proceedings of 27th Asilomar Conference on Signals, Systems and Computers* (1993), pp. 40–44 vol.1, doi: [mu10.1109/ACSSC.1993.342465](https://doi.org/10.1109/ACSSC.1993.342465), iSSN: 1058-6393.

<sup>8</sup>Y. Chi, L. L. Scharf, A. Pezeshki, and A. R. Calderbank, “Sensitivity to Basis Mismatch in Compressed Sensing,” *IEEE Transactions on Signal Processing* **59**(5), 2182–2195 (2011) doi: [mu10.1109/TSP.2011.2112650](https://doi.org/10.1109/TSP.2011.2112650).

<sup>9</sup>V. Duval and G. Peyré, “Sparse regularization on thin grids I: the Lasso,” *Inverse Problems* **33**(5), 055008 (2017) doi: [mu10.1088/1361-6420/aa5e12](https://doi.org/10.1088/1361-6420/aa5e12).

<sup>10</sup>C. Ekanadham, D. Tranchina, and E. P. Simoncelli, “Recovery of Sparse Translation-Invariant Signals With Continuous Basis Pursuit,” *IEEE Transactions on Signal Processing* **59**(10), 4735–4744 (2011) doi: [mu10.1109/TSP.2011.2160058](https://doi.org/10.1109/TSP.2011.2160058) conference Name: *IEEE Transactions on Signal Processing*.

<sup>11</sup>Y. Park, W. Seong, and P. Gerstoft, “Block-sparse two-dimensional off-grid beamforming with arbitrary planar array geometry,” *The Journal of the*

- Acoustical Society of America **147**(4), 2184–2191 (2020) [muhttp://asa.scitation.org/doi/10.1121/10.0000983](http://asa.scitation.org/doi/10.1121/10.0000983) doi: [mu10.1121/10.0000983](https://doi.org/10.1121/10.0000983).
- <sup>12</sup>Z. Yang, L. Xie, and C. Zhang, “Off-Grid Direction of Arrival Estimation Using Sparse Bayesian Inference,” *IEEE Transactions on Signal Processing* **61**(1), 38–43 (2013) doi: [mu10.1109/TSP.2012.2222378](https://doi.org/10.1109/TSP.2012.2222378) conference Name: IEEE Transactions on Signal Processing.
- <sup>13</sup>A. Das, “Deterministic and Bayesian Sparse Signal Processing Algorithms for Coherent Multipath Directions-of-Arrival (DOAs) Estimation,” *IEEE Journal of Oceanic Engineering* 1–15 (2018) doi: [mu10.1109/JOE.2018.2851119](https://doi.org/10.1109/JOE.2018.2851119).
- <sup>14</sup>A. Xenaki and P. Gerstoft, “Grid-free compressive beamforming,” *The Journal of the Acoustical Society of America* **137**(4), 1923–1935 (2015) [muhttp://asa.scitation.org/doi/10.1121/1.4916269](http://asa.scitation.org/doi/10.1121/1.4916269) doi: [mu10.1121/1.4916269](https://doi.org/10.1121/1.4916269) publisher: Acoustical Society of America.
- <sup>15</sup>Y. Yang, Z. Chu, Z. Xu, and G. Ping, “Two-dimensional grid-free compressive beamforming,” *The Journal of the Acoustical Society of America* **142**(2), 618–629 (2017) [muhttp://asa.scitation.org/doi/10.1121/1.4996460](http://asa.scitation.org/doi/10.1121/1.4996460) doi: [mu10.1121/1.4996460](https://doi.org/10.1121/1.4996460) publisher: Acoustical Society of America.
- <sup>16</sup>Y. Park, Y. Choo, and W. Seong, “Multiple snapshot grid free compressive beamforming,” *The Journal of the Acoustical Society of America* **143**(6), 3849–3859 (2018) [muhttp://asa.scitation.org/doi/10.1121/1.5042242](http://asa.scitation.org/doi/10.1121/1.5042242) doi: [mu10.1121/1.5042242](https://doi.org/10.1121/1.5042242) publisher: Acoustical Society of America.
- <sup>17</sup>E. J. Candès and C. Fernandez-Granda, “Towards a Mathematical Theory of Super-resolution,” *Communications on Pure and Applied Mathematics* **67**(6), 906–956 (2014) [muhttp://onlinelibrary.wiley.com/doi/abs/10.1002/cpa.21455](http://onlinelibrary.wiley.com/doi/abs/10.1002/cpa.21455) doi: [muhttps://doi.org/10.1002/cpa.21455](https://doi.org/10.1002/cpa.21455) eprint: <https://onlinelibrary.wiley.com/doi/pdf/10.1002/cpa.21455>.
- <sup>18</sup>C. Fernandez-Granda, “Super-resolution of point sources via convex programming,” *Information and Inference: A Journal of the IMA* **5**(3), 251–303 (2016) [muhttps://doi.org/10.1093/imaiai/iaw005](https://doi.org/10.1093/imaiai/iaw005) doi: [mu10.1093/imaiai/iaw005](https://doi.org/10.1093/imaiai/iaw005).
- <sup>19</sup>Z. Chu, Y. Liu, Y. Yang, and Y. Yang, “A preliminary study on two-dimensional grid-free compressive beamforming for arbitrary planar array geometries,” *The Journal of the Acoustical Society of America* **149**(6), 3751–3757 (2021) [muhttps://asa.scitation.org/doi/10.1121/10.0005059](https://asa.scitation.org/doi/10.1121/10.0005059) doi: [mu10.1121/10.0005059](https://doi.org/10.1121/10.0005059).
- <sup>20</sup>B. Mamandipoor, D. Ramasamy, and U. Madhow, “Newtonized Orthogonal Matching Pursuit: Frequency Estimation Over the Continuum,” *IEEE Transactions on Signal Processing* **64**(19), 5066–5081 (2016) doi: [mu10.1109/TSP.2016.2580523](https://doi.org/10.1109/TSP.2016.2580523) conference Name: IEEE Transactions on Signal Processing.
- <sup>21</sup>Y. Yang, Z. Chu, Y. Yang, and S. Yin, “Two-dimensional Newtonized orthogonal matching pursuit compressive beamforming,” *The Journal of the Acoustical Society of America* **148**(3), 1337–1348 (2020) [muhttp://asa.scitation.org/doi/10.1121/10.0001919](http://asa.scitation.org/doi/10.1121/10.0001919) doi: [mu10.1121/10.0001919](https://doi.org/10.1121/10.0001919) publisher: Acoustical Society of America.
- <sup>22</sup>Y. de Castro and F. Gamboa, “Exact reconstruction using Beurling minimal extrapolation,” *Journal of Mathematical Analysis and Applications* **395**(1), 336–354 (2012) [muhttps://www.sciencedirect.com/science/article/pii/S0022247X12003952](https://www.sciencedirect.com/science/article/pii/S0022247X12003952) doi: [mu10.1016/j.jmaa.2012.05.011](https://doi.org/10.1016/j.jmaa.2012.05.011).
- <sup>23</sup>Q. Denoyelle, V. Duval, G. Peyré, and E. Soubies, “The sliding Frank–Wolfe algorithm and its application to super-resolution microscopy,” *Inverse Problems* **36**(1), 014001 (2019) [muhttps://doi.org/10.1088/1361-6420/ab2a29](https://doi.org/10.1088/1361-6420/ab2a29) doi: [mu10.1088/1361-6420/ab2a29](https://doi.org/10.1088/1361-6420/ab2a29) publisher: IOP Publishing.
- <sup>24</sup>G. Battista, P. Chiariotti, M. Martarelli, and P. Castellini, “Inverse methods in aeroacoustic three-dimensional volumetric noise source localization and quantification,” *Journal of Sound and Vibration* **473**, 115208 (2020) [muhttp://www.sciencedirect.com/science/article/pii/S0022460X20300390](http://www.sciencedirect.com/science/article/pii/S0022460X20300390) doi: [mu10.1016/j.jsv.2020.115208](https://doi.org/10.1016/j.jsv.2020.115208).
- <sup>25</sup>F. Ning, J. Wei, L. Qiu, H. Shi, and X. Li, “Three-dimensional acoustic imaging with planar microphone arrays and compressive sensing,” *Journal of Sound and Vibration* **380**, 112–128 (2016) [muhttps://www.sciencedirect.com/science/article/pii/S0022460X16302310](https://www.sciencedirect.com/science/article/pii/S0022460X16302310) doi: [mu10.1016/j.jsv.2016.06.009](https://doi.org/10.1016/j.jsv.2016.06.009).
- <sup>26</sup>T. Padois and A. Berry, “Two and Three-Dimensional Sound Source Localization with Beamforming and Several Deconvolution Techniques,” *ACTA ACUSTICA UNITED WITH ACUSTICA* **103**, 10 (2017).
- <sup>27</sup>G. Chardon and U. Boureau, “gilleschardon/SFWCB” doi:10.5281/zenodo.5528801 <https://zenodo.org/record/5528801> last accessed 26/09/2021.
- <sup>28</sup>J. Chen and X. Huo, “Theoretical Results on Sparse Representations of Multiple-Measurement Vectors,” *IEEE Transactions on Signal Processing* **54**(12), 4634–4643 (2006) doi: [mu10.1109/TSP.2006.881263](https://doi.org/10.1109/TSP.2006.881263) conference Name: IEEE Transactions on Signal Processing.
- <sup>29</sup>V. Duval and G. Peyré, “Sparse spikes super-resolution on thin grids II: the continuous basis pursuit,” *Inverse Problems* **33**(9), 095008 (2017) [muhttps://doi.org/10.1088/1361-6420/aa7fce](https://doi.org/10.1088/1361-6420/aa7fce) doi: [mu10.1088/1361-6420/aa7fce](https://doi.org/10.1088/1361-6420/aa7fce).

- <sup>30</sup>Technically a member of a  $\sigma$ -algebra of  $\Omega$ . For sake of clarity, such technicalities will not be considered here, and are discussed at length in appropriate textbooks<sup>31</sup>.
- <sup>31</sup>W. Rudin, *Real and Complex Analysis, 3rd Ed.* (McGraw-Hill, Inc., USA, 1987).
- <sup>32</sup>J. Nocedal and S. J. Wright, *Numerical Optimization, 2nd Ed.* (Springer, 2006) chapter 18.
- <sup>33</sup>J.-B. Courbot and B. Colicchio, “A fast homotopy algorithm for gridless sparse recovery,” *Inverse Problems* **37**(2), 025002 (2021) doi: [mu10.1088/1361-6420/abd29c](https://doi.org/10.1088/1361-6420/abd29c) publisher: IOP Publishing.
- <sup>34</sup>O. Scherzer, “The use of Morozov’s discrepancy principle for Tikhonov regularization for solving nonlinear ill-posed problems,” *Computing* **51**(1), 45–60 (1993) [muhttps://doi.org/10.1007/BF02243828](https://doi.org/10.1007/BF02243828) doi: [mu10.1007/BF02243828](https://doi.org/10.1007/BF02243828).
- <sup>35</sup>G. Chardon, F. Ollivier, and J. Picheral, “Localization of sparse and coherent sources by orthogonal least squares,” *The Journal of the Acoustical Society of America* **146**(6), 4873–4882 (2019) [muhttp://asa.scitation.org/doi/10.1121/1.5138931](http://asa.scitation.org/doi/10.1121/1.5138931) doi: [mu10.1121/1.5138931](https://doi.org/10.1121/1.5138931) publisher: Acoustical Society of America.